UC Berkeley
UC Berkeley Previously Published Works

Title
Ecomorphodynamic approaches to river anabranching patterns

Permalink
https://escholarship.org/uc/item/4mw2m1qr

Authors
Crouzy, Benoît
Bärenbold, Fabian
D'Odorico, Paolo
et al.

Publication Date
2016-07-01

DOI
10.1016/j.advwatres.2015.07.011

Peer reviewed

eScholarship.org Powered by the California Digital Library
University of California

Advances in Water Resources 93 (2016) 156–165

Contents lists available at ScienceDirect

Advances in Water Resources

journal homepage: www.elsevier.com/locate/advwatres

Ecomorphodynamic approaches to river anabranching patterns

Benoît Crouzy [a,*], Fabian Bärenbold [a], Paolo D'Odorico [b], Paolo Perona [a]

[a] Group of Applied HydroEconomics and Alpine Environmental Dynamics, IEE, EPFL-ENAC, Station 2, Lausanne, CH 1015, Switzerland
[b] Department of Civil and Environmental Engineering, University of Virginia, Charlottesville, USA

ARTICLE INFO

Article history:
Available online 21 July 2015

Keywords:
Riparian vegetation
Physical model
Neural model
Stability analysis

ABSTRACT

We investigate the influence of vegetation on river morphological instabilities using an analytical framework. We first discuss the important role of the hydrological (flooding frequency) and biological (vegetation development rate) timescales. As long as the changes in riverbed morphology and vegetation over an interval comprising one flood and one low-flow period are small, we show that it is possible to simplify the description of a vegetated river with non-constant discharge. We propose physically-based and effective (neural) models for the feedback between vegetation and morphodynamics. Physically-based approaches use equations of morphodynamics extended to account for the interplay between flow, sediment and vegetation dynamics. While their foundation is solid, a physically-based description is only feasible for simple vegetation cover (grass to shrubs). For complex vegetated obstacles we present as an alternative effective approaches, explicitly including interactions (local and non-local) between obstacles. We focus on the role of vegetation in the emergence of ridge patterns observed in the presence of an ephemeral flow and correspondingly derive a set of conditions for patterns.

© 2015 Elsevier Ltd. All rights reserved.

1. Introduction

Riparian vegetation and its couplings to river morphological evolution have recently triggered an increased research activity: field studies [1], laboratory experiments [2,3] and models [4,5] have shed a new light on the complexity of the feedback between biological and morphological processes. There has been a change of paradigm [6,7] in the description and modeling of riparian vegetation, going from the view of vegetation as a static element part of a classic hydraulic model [8,9] to a more complex viewpoint where vegetation dynamics is fully considered [6,10–13]. The historical tendency to either neglect the presence of biomass in rivers or disregard its dynamical character was the expression of the difficulty to present a comprehensive framework and account for all the ecological and geomorphological processes occurring within the river (eco)system.

While recent research (for a review, see [1,4]) has partly filled this gap, stability analysis of morphological equations [14] including the dynamics of vegetation and the feedback between biological and river processes (flow and sediment) has not been explored yet. Classically, linear stability analysis of morphological equations has been a tool of choice for explaining universal river features. We shall not attempt a comprehensive review here but one may cite for example works on the instability toward ripples and (anti-) dunes [15], alternate/multiple bars [16] and meanders [17–19].

In this work, we use classic stability analysis in order to study the emergence of vegetated patterns in two models for the evolution of riparian vegetation. We begin with a physically-based approach in the form of an extension of standard morphological equations [14] (shallow water equations + Exner) to include the evolution of vegetation and the feedback between riparian vegetation and river morphodynamics. The use of a physically-based description is feasible only for the most simple situations. We therefore propose the alternative of using a lumped model for the evolution of the biomass, which allows us to include effects such as scouring around a vegetated patch (increased local velocity and/or turbulent kinetic energy, denoted TKE hereafter) or the presence of a sediment tail behind a permeable vegetated obstacle [20,21]. As case study, we focus on the role of vegetation in the formation of anabranching ridge patterns observed in various fluvial environments.

In Fig. 1, we present two contrasting examples for such patterns, corresponding to the simple vegetation cover and the more complex vegetated obstacles mentioned above. Anabranching patterns (Fig. 1, upper panel) consisting of stable ridges dividing the main channel were described in the Marshall River [22–24] (Australia, NT) and the formation of those patterns was explained using classic hydraulic arguments (optimization of the bedload transport capacity) [25,26] or conceptual models [22,27]. In the lower panel of Fig. 1 we show rills observed on a river bar of the Thur River (Switzerland). The type of vegetation cover is very different in the two rivers: in the

* Corresponding author. Tel.: +41 797048633.
E-mail address: crouzy@gmail.com, benoit.crouzy@epfl.ch, benoit.crouzy@a3.epfl.ch (B. Crouzy).

http://dx.doi.org/10.1016/j.advwatres.2015.07.011
0309-1708/© 2015 Elsevier Ltd. All rights reserved.

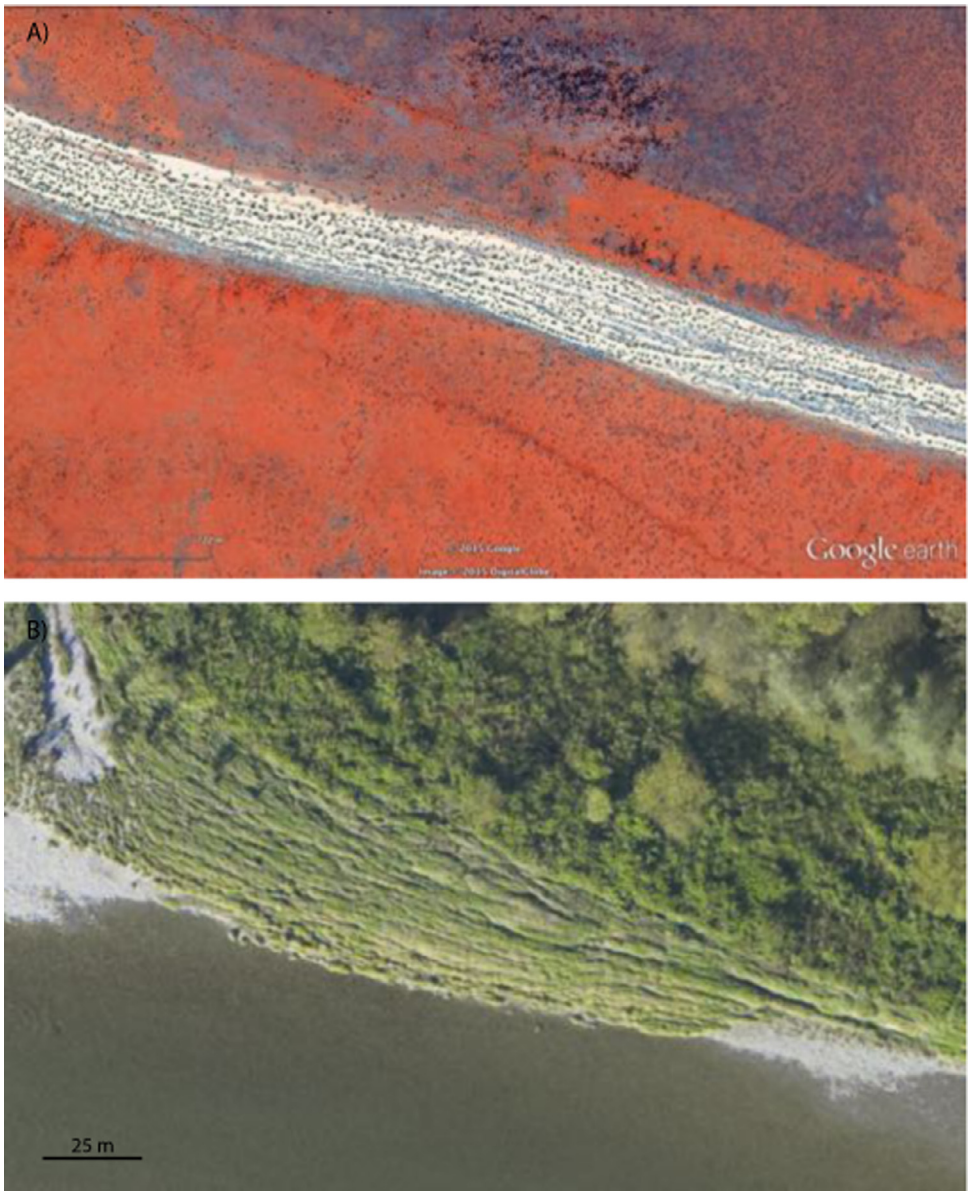

Fig. 1. Examples of anabranching patterns emerging in two contrasting fluvial environments: (A) anabranching of the entire river bed (Marshall River, Australia, NT) and (B) rills observed on a bar of the Thur River, Switzerland.

Marshall river we have well-developed tall-shrubs and trees (teatrees and river red gums), while grass grows on the bar depicted in the lower panel of Fig. 1. Common to those two environments is the presence of an ephemeral flow resulting either from the ephemeral character of the river (Marshall River) or the position (elevated bar) within the riverbed (Thur River). Another similitude is the presence of low cohesive sediment causing significant biomass mortality. The ephemeral flow allows for a feedback loop between ecological and morphological processes: changes in riverbed morphology are typically faster than the development of vegetation but are only taking place during flow events. As suggested by [13] and empirically investigated by [3,28], the feedback loop is only observed for a certain window of ratios between the frequency of flooding events and the development rate of vegetation. For too rare flooding events the vegetation grows out of scale compared to the uprooting capacity of the floods. Conversely, very frequent events completely uproot all the vegetation present in the channel.

The paper is organized as follows: in the next Section we show how it is possible under certain assumptions to reduce the description of the vegetation dynamics in the presence of a variable discharge to an equivalent situation with constant flow; in Section 3 we present the stability analysis of a physically-based ecomorphodynamic model for the emergence of vegetated river patterns, focusing on the asymmetry of the patterns; in Section 4 we present an effective model that allows us to describe the interactions among complex vegetated obstacles in a river; we then perform the stability analysis of this model; in Section 5 we discuss our results and the domain of validity for the two approaches we propose; finally, Section 6 concludes the work.

2. Hydrological and biological timescales

Before turning to the modeling framework for the feedback between the evolution of the biomass and the morphodynamics (flow and sediment dynamics), we discuss here the important role of the characteristic timescales for the biological and hydrological processes. In typical field situations, one observes that the dynamics of vegetation development is much slower than the morphodynamics.

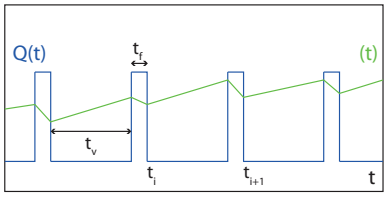

Fig. 2. Idealized river hydrograph $Q(t)$ (blue curve) with t_f the flood duration and t_v the inter-event time between flooding events, together with the schematic evolution of the biomass density $\phi(t)$ (green curve) accounting for mortality during flooding events. (For interpretation of the references to color in this figure legend, the reader is referred to the web version of this article.)

In turn, morphological changes occur over a much longer timescale than changes of local flow conditions. This hierarchy of timescales has led people to try capturing the effect of riparian vegetation without considering its dynamics, for example by a change in channel roughness [9,29]. Motivated by experimental findings [3,28,30], we show here that a complete feedback loop can however be observed due to the non-constant flow characterizing typical river hydrographs. The flow-induced mortality is indeed only active during flooding events while vegetation can in principle develop over a longer period (albeit very slowly). It is correspondingly possible to define an optimal window of inter-event times between flooding events characterized by a strongly coupled co-evolution of vegetation and riverbed morphology.

Mathematically, the situation described above can be modeled by writing an equation for the evolution of the biomass over a period going from the end of one flooding event to the end of the subsequent flooding event. To fix ideas, let us begin with a simplified periodic hydrograph (Fig. 2) consisting of periods t_v with no flow-associated mortality where the biomass can evolve unhindered, followed by flooding events of short duration t_f and constant flow. We introduce in addition $\phi_i = \phi(t_i)$ the local biomass density at the end of a given flooding event i. Assuming that the biomass density does not vary too fast, we can write a finite-difference equation for the evolution of the biomass

$$\Delta\phi_i = \phi_{i+1} - \phi_i = t_v(\alpha_g\phi_i(\phi_m - \phi_i) + D\nabla^2\phi_i) - t_f F(\phi_i, \mathbf{U}_i, Y_i). \tag{1}$$

Throughout Eq. (1) the index i refers to quantities taken at a time t_i. The first term in the right-hand side describes growth (logistic) and spreading (diffusion coefficient D) of the biomass. We assume growth to follow a logistic dependence [31], which is characterized by an exponential growth (rate α_g) in the initial stage, followed by a slower growth until the maximal carrying capacity ϕ_m is obtained. The second term describes mortality through the function F depending on local flow velocity $\mathbf{U}_i$ and flow depth Y_i. For the sake of keeping the discussion as general as possible, we will leave F unspecified throughout this Section and fix it only in the following Sections. We want to stress on the fact that Eq. (1) is valid in the limit of slow-changing biomass, which can be formulated mathematically as

$$\frac{\Delta\phi_i}{\phi_i} \ll 1. \tag{2}$$

Dividing both sides of Eq. (1) by the duration of one cycle $t_v + t_f$, one obtains a partial differential equation for the evolution of the biomass

$$\frac{\partial\phi}{\partial t} = r_g\big(\alpha_g\phi(\phi_m - \phi) + \nabla^2\phi\big) - r_d F(\phi, \mathbf{U}, Y), \tag{3}$$

where we have introduced the ratios $r_g = \frac{t_v}{t_v+t_f} \sim 1$ and $r_d = \frac{t_f}{t_v+t_f} \ll 1$. We have thus reduced the equation for the evolution of the biomass density under non-constant flow to an effective equation where low-flow periods have been suppressed. Those long periods with no flow-induced mortality result however in an increased growth rate of vegetation, which may become comparable to the mortality term. For the right ratio between the timescales one can observe an interplay between the evolution of the vegetation and the morphodynamics due to the factors r_g and r_d that compensate for the fact that usually the evolution of the vegetation is much slower than the river morphodynamics. However, if the ratio r_d/r_g is too small, then vegetation can grow out of scale compared to the erosive capacity of the floods. In the opposite limit of $r_g \sim r_d$ the flooding events completely wipe out the vegetation cover over each flooding event.

As long as condition (2) is satisfied, we can generalize our method to the situation with a non-periodic hydrograph. However, in this case, the ratios between the timescales r_g and r_d become time dependent. Formally, this is expressed by the need of introducing $r^i_{g,d}$ in Eq. (3) to account for the variable duration of the flooding events and of the inter-event time between two floods.

In Sections 3 and 4 we shall use a constant flow description valid under the premise that the assumption (2) on the magnitude of the biomass changes over a cycle is satisfied.

3. Physically-based equations

As a first step, it is natural to try approaching the interplay between ecological and morphodynamical processes using a physically-based description. For the time being, we consider a simplified generic problem, involving model vegetation and disregarding complications like the sorting of sediment according to the grain size. We shall consider here the situation with a shallow flow in a straight rectangular channel, which allows us to simplify the Navier–Stokes equations by integrating out the dependence of the flow velocity along the vertical direction. The equations we introduce below are similar to the ones proposed by [32] for a converging narrow channel (one-dimensional description of the flow). We describe vegetation by the presence of rigid emerging cylindrical obstacles (diameter d and drag coefficient c_D) whose density (evolving according to the time t) is given by a field $\phi(s, n, t)$. Hereafter, the variables s and n denote the streamline and transverse coordinates respectively. The channel bed is mobile, and its elevation is given by the field $\eta(s, n, t)$. We begin by writing the equations for momentum conservation

$$\frac{\partial U}{\partial t} = -U\frac{\partial U}{\partial s} - V\frac{\partial U}{\partial n} - g\left[\frac{\partial Y}{\partial s} + \frac{\partial \eta}{\partial s}\right] - \frac{g}{Y}\left[\frac{1}{\chi_b^2} + \frac{c_D d Y \phi}{2g}\right]U||\mathbf{U}|| \tag{4a}$$

$$\frac{\partial V}{\partial t} = -U\frac{\partial V}{\partial s} - V\frac{\partial V}{\partial n} - g\left[\frac{\partial Y}{\partial n} + \frac{\partial \eta}{\partial n}\right] - \frac{g}{Y}\left[\frac{1}{\chi_b^2} + \frac{c_D d Y \phi}{2g}\right]V||\mathbf{U}||. \tag{4b}$$

Here the flow is given by the vector $\mathbf{U} = (U, V)$ with $U(s, n, t)$ the component of the flow in the streamline direction $\mathbf{e}_s$ and $V(s, n, t)$ the component transverse to the flow (coordinate axis $\mathbf{e}_n$). Flow depth is given by the variable $Y(s, n, t)$. We use the Chezy formula as closure relation for the momentum equation, as modified by [29] to include the roughness induced by rigid vegetation in addition to the bed roughness (friction coefficient without vegetation χ_b, related to the Strickler coefficient k_{st}). Next, we write the equation for mass conservation

$$\frac{\partial Y}{\partial t} = -\nabla\cdot(Y\mathbf{U}). \tag{5}$$

Note that we disregard here for simplicity the volume of the biomass, assuming that the cross-section of the biomass is much smaller than the river cross-section. In order to describe sediment transport in the form of bed load we use the Exner equation

$$\frac{\partial \eta}{\partial t} = -\frac{\nabla\cdot\mathbf{Q_s}}{(1-p)}, \tag{6}$$

with $\mathbf{Q_s}$ the sediment flux and p the porosity of the riverbed. In addition, for the sake of obtaining analytical results, we shall use (following [33]) a simplified closure relation for sediment transport

$$\mathbf{Q_s} = a||\mathbf{U}||^m\mathbf{e}. \tag{7}$$

with $\mathbf{e}$ a unit vector giving the direction of the sediment flux from flow velocity and a correction accounting for the transverse slope gradient

$$\mathbf{e} = \left(U/||\mathbf{U}||, V/||\mathbf{U}|| - \frac{r}{\sqrt{\tau_*}}\frac{\partial \eta}{\partial n}\right). \tag{8}$$

In addition, we have introduced $0.5 \lesssim r \lesssim 0.6$ an empirical parameter following [17] and the dimensionless Shields stress τ_* (for more details see [34]). The use of the simplified description (7) is justified when working in the limit of well-developed sediment transport, always above the critical bed shear stress for the onset of sediment transport. In the following, we shall use the well-known formula by [35], which leads, after taking the limit of well-developed sediment transport, to $m = 3$. Finally, in order to express the fact that the characteristic timescale for morphological processes is much slower than the timescale for the flow dynamics [14], we express the parameter a indirectly via the dimensionless parameter $\gamma = \frac{3Q_{s0}}{(1-p)Y_0U_0} \ll 1$, where the subscripts 0 indicate quantities taken under normal flow conditions. The equation for the evolution of the biomass needs to be discussed in greater details. We assume the biomass to evolve following:

$$\frac{\partial \phi}{\partial t} = \alpha_g\phi(\phi_m - \phi) + D\nabla^2\phi - \alpha_d Y\mathbf{U}^2\phi, \tag{9}$$

where the field $\phi(s, n, t)$ gives the time-dependent density of plants per unit area. As in the previous Section, we assume the evolution of the biomass to follow a logistic dependence with carrying capacity ϕ_m. The second term in the right-hand side of Eq. (9) describes the spreading of the biomass by a diffusion term [36,37]. For a detailed discussion on how diffusion can be seen as the generic form of positive local feedback on biomass growth, see Section 4. Here again, we choose to restrict ourselves to a simple situation in order to obtain an analytically tractable model: we do not consider effects such as the dependence of the growth rate on the position in the channel (water availability) or the competition between different riparian species [38]. We introduce, however, the influence of local flow conditions on the evolution of the biomass in the form of a mortality term proportional to the rate of momentum transfer from flow to vegetation (third term in the right-hand side of Eq. (9)).

Before turning to the analysis of our ecomorphodynamic equations (4)–(9), we want to stress on the fact that, while we have introduced simplifications in the model formulation, the methodology we use can readily be generalized. One exception in this regard is including explicitely a critical threshold for the onset of sediment transport present in several closure relations [35,39], which would preclude using our analytical framework (discontinuity in the derivative).

In order to discuss the appearance of vegetated anabranching patterns, we perform a stability analysis of the ecomorphodynamic model (4)–(9). We shall not describe here in details the procedure of stability analysis: the method and the Ansatz by [33] can readily be applied to our model. The idea is to start from the homogeneous solution of Eqs. (4)–(9), which we denote $\mathbf{X}_0 = (U_0, V_0, Y_0, \eta_0, \phi_0)$. Perturbing a state with a strictly positive biomass density (well-developed vegetation cover) is essential: a perturbation around $\phi_0 = 0$ would result in (non-physical) negative vegetation densities. For the sake of self-consistency we give here the functions which are used to perturbate the homogeneous state:

$$[(U_1, V_1\tan(k_n n + \psi), Y_1, \eta_1, \phi_1)\cos(k_n n + \psi) \times \exp(ik_s s + \omega t) + cc.], \tag{10}$$

where $cc.$ denotes the complex conjugate. We have introduced ω, the growth rate of a perturbation with given transverse and longitudinal wavenumbers k_n and k_s respectively (wavelengths are given by $\lambda_{s,n} = \frac{2\pi}{k_{s,n}}$). In the transverse direction the wavenumber k_n is restricted to the values $\frac{\pi m}{W}$, with W the channel width, in order to satisfy the zero-flow condition at the river boundary $V(\pm W/2 = 0)$. For odd values of m we have $\psi = \frac{\pi}{2}$, while for even values of m the dephasing ψ is zero. The variable m gives the order of the bars in the transverse direction: $m = 1$ corresponds to alternate bars and $m > 1$ to multiple bars. In the longitudinal direction the wavenumber can take arbitrary real values, which amounts to assuming an infinite channel. In Fig. 3 we present an example where the river dynamics result in the formation of vegetated multiple bars. Applying the perturbation Ansatz (10) to Eqs. (4)–(9) and keeping only the first order term of the perturbation expansion allows us to reduce the ecomorphodynamic problem to the following problem:

$$\frac{\partial \mathbf{X}_1}{\partial t} = A\mathbf{X}_1, \tag{11}$$

with $\mathbf{X}_1 = (U_1, V_1, Y_1, \eta_1, \phi_1)$, and A a 5×5 matrix depending on the model parameters (see Eqs. (4)–(9)) and on the wavenumbers k_n and k_s. We search for eigenvectors in the form

$$A\mathbf{X}_1 = \omega\mathbf{X}_1. \tag{12}$$

The mode which is the most unstable (i.e. with the largest ω) is going to dominate. However, if no mode satisfies the condition $\omega > 0$, the homogeneous solution $\mathbf{X}_0$ is stable and the channel does not evolve towards patterns. In principle it is possible to have a system homogeneous in the transverse direction ($m = 0$) presenting patterns

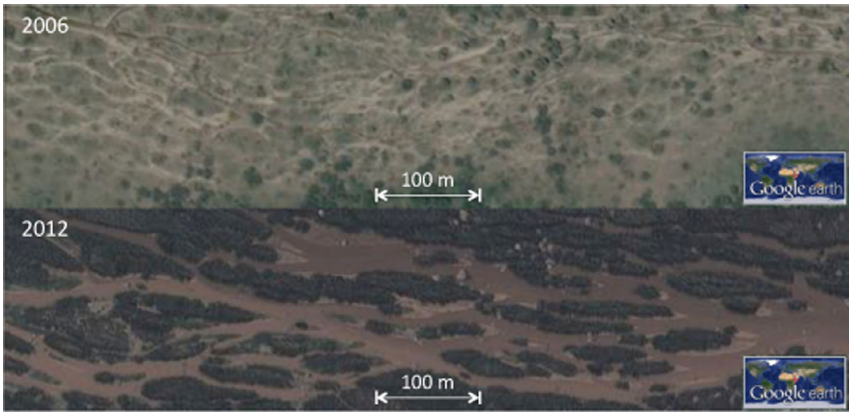

Fig. 3. Evolution of the floodplain of the Awash River, Ethiopia, Afar Region (11°27′0.56″N 40°58′0.29″E) from 2006 (upper panel) to 2012 (lower panel). Map data: Google, Digitalglobe.

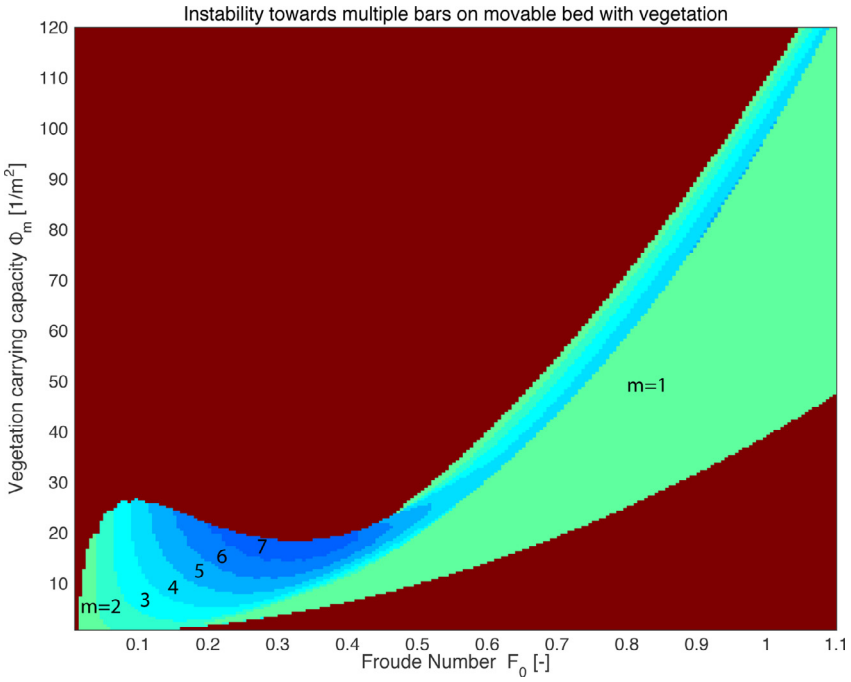

Fig. 4. Instability towards multiple bars varying the Froude number and the carrying capacity of the biomass. Darker blue colors correspond to increasing the order of the bars in the transverse direction ($m = 2 - 7$). The domain in green indicates instability towards alternate bars ($m = 1$). The red color indicates no instability towards patterns. Fixed parameters: vegetation stem diameter $d = 0.01$ m, sediment grain diameter $d_s = 0.001$ m, channel aspect ratio $\beta = 80$, normal water depth $Y_0 = 1$ m, biomass growth rate $\alpha_g = 0.25\,\mathrm{m^2\,s^{-1}}$, biomass mortality rate $\alpha_d = 0.25\,\mathrm{m^{-3}\,s^{-1}}$, Stokes drag coefficient $c_D = 1.5$, transverse slope parameter $r = 0.5$, vegetation diffusion coefficient $D = 100\,\mathrm{m^2\,s^{-1}}$, dimensionless parameter $\gamma = 10^{-3}$ and Strickler coefficient $k_{st} = 33.33\,\mathrm{m^{1/3}\,s^{-1}}$. (For interpretation of the references to color in this figure legend, the reader is referred to the web version of this article.)

in the longitudinal direction ($k_s > 0$). Although we are mainly interested in two-dimensional effects in this work, we refer here to [16] for a study on the one-dimensional problem (without vegetation). Note finally that we shall not discuss here effects related to the non-normality of the operator A. As shown by [40], while the morphodynamical equations evolve asymptotically toward the most unstable mode of our perturbation Ansatz (10), a non-monotonic evolution of the disturbances can be observed at finite times.

We focus here on the asymmetry between the longitudinal and the transverse length scale of the patterns: the anabranching patterns we investigate in this work are typically characterized by the coalescing of island into ridges presenting a large length-to-width ratio. For example, considering the situation in the Marshall River (upper panel of Fig. 1), one obtains a ratio larger than 10 [22,23]. The systematic stability analysis of the ecomorphodynamic model goes beyond the scope of this work and will be presented elsewhere [41]. In Fig. 4, we present domains of instability with non-zero biomass density, colored according to the order of the bars corresponding to the most unstable mode, varying the Froude number $F_0 = \frac{U_0}{\sqrt{gY_0}}$ and the vegetation carrying capacity ϕ_m. The set of fixed parameters in Fig. 4 has been chosen in order to observe an instability domain representative of all the possible features (alternate/multiple bars, low/high asymmetry and instability driven by vegetation dynamics and/or sediment dynamics). The role of the different parameters needs to be discussed individually. Regarding the diffusion coefficient D, the stronger the diffusion, the longer the pattern wavelength (and the smaller the order of the bars). The role of the growth coefficient α_g is qualitatively similar to the role of the carrying capacity. Finally, a small β would preclude the appearance of (multiple) bars and a too strong uprooting coefficient α_d would reduce the dynamics to its flow and sediment components. Note that we work in the limit of a large aspect ratio $\beta = W/(2Y_0)$ in order to observe two dimensional structures. One readily notices that for a large carrying capacity the presence of vegetation favors configurations with $m \leq 1$ (in some regions an increase in the carrying capacity can however lead to an increasing bar order). Interestingly, this stabilization towards a single-threaded channel (homogeneous solution or alternate bars) is observed without introducing any bank stabilization by vegetation in the model. A similar result is obtained when plotting the instability domains as a function of the vegetation growth rate α_g (not reproduced here). This is consistent with the findings by [42] on the association between the expansion of vegetation during the Carboniferous and the evolution of anabranching channels towards single-threaded channels (recall that the instability toward alternate bars is the first step toward meandering instability [18]). In Fig. 5, we color the instability domains of Fig. 4 according to the asymmetry (k_n/k_s) of the patterns. Remarkably, we can hardly identify domains with instability towards multiple bars *and* an asymmetry $k_n/k_s > 5$. Fig 5 corresponds to the choice of realistic model parameters amounting for the strongest asymmetry. As a consequence, we conclude that, while the physically-based approach allows us to capture the channel stabilizing effect by vegetation, it is not sufficient to describe the formation of stable ridges dividing the main channel as observed in [22,23] and represented in the upper panel of Fig. 1. Note however that we cannot exclude a correction in the pattern wavelength and asymmetry if the perturbation grows up to the point where nonlinear effects become important.

In the next Section, we show that by introducing more complex non-local interactions between vegetated obstacles located at different points in the channel we are able to reproduce the organization of the vegetation cover in stable ridges.

4. Kernel-based approach

The idea of the Kernel approach (also denoted “neural model” [36]) is to write a lumped equation for the evolution of the biomass including the interactions between vegetated obstacles. Those interactions originate from flow disturbances by the biomass (resulting in turn in characteristic sediment patterns around obstacles). Note also

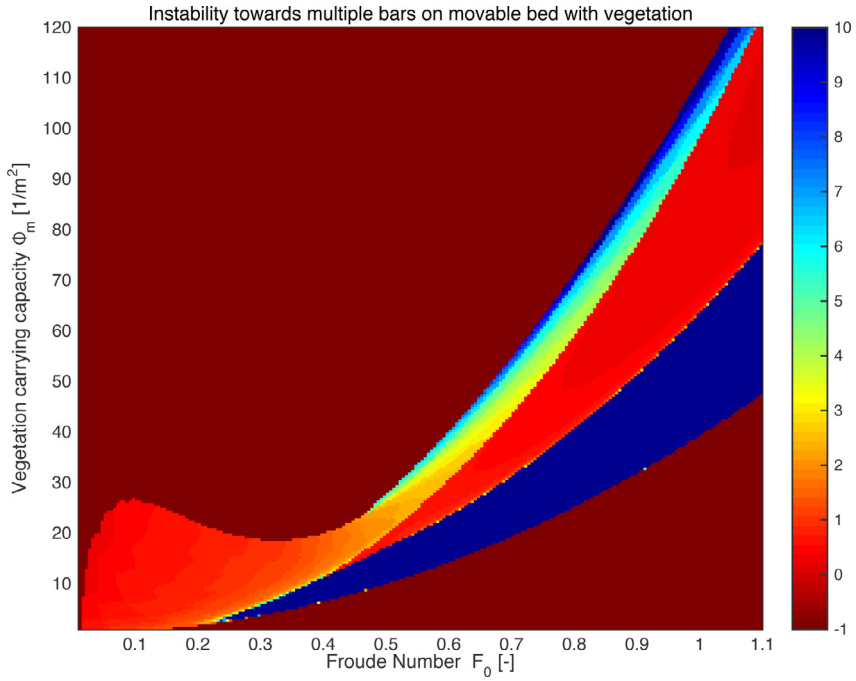

Fig. 5. Asymmetry $k_n/k_s = \lambda_s/\lambda_n$ between the longitudinal wavelength λ_s and the transverse wavelength λ_n of the most unstable mode. Negative values indicate no instability towards patterns. Fixed parameters: vegetation stem diameter $d = 0.01$ m, sediment grain diameter $d_s = 0.001$ m, channel width-to-depth ratio $\beta = 80$, normal water depth $Y_0 = 1$ m, biomass growth rate $\alpha_g = 0.25\,\mathrm{m^2\,s^{-1}}$, biomass mortality rate $\alpha_d = 0.25\,\mathrm{m^{-3}\,s^{-1}}$, Stokes drag coefficient $c_D = 1.5$, transverse slope parameter $r = 0.5$, vegetation diffusion coefficient $D = 100\,\mathrm{m^2\,s^{-1}}$, dimensionless parameter $\gamma = 10^{-3}$ and Strickler coefficient $k_{st} = 33.33\,\mathrm{m^{1/3}\,s^{-1}}$.

that although we try to present a comprehensive review here, more details on the Kernel model can be found in [43]. In its generic form, a Kernel model for the dynamics of the biomass density $\phi(s, n, t)$ can be written as a convolution

$$\frac{\partial \phi}{\partial t} = \alpha_g \phi(\phi_m - \phi) + \iint \phi(s', n', t)\mathcal{W}(s' - s, n' - n)ds'dn'. \quad (13)$$

As in Eq. (9) from the previous Section, we recover the standard logistic growth of biomass, where α_g denotes the growth rate and ϕ_m the carrying capacity. The difference with the physically-based approach lies in the interaction Kernel $\mathcal{W}$, which does not contain explicitly any information on the local flow conditions. This contrasts with the approach of the previous Section, where biomass mortality was related to the rate of momentum transfer from the flow to the vegetation. However, although the loss of the explicit coupling with the dynamics of the flow and sediment may appear as a drawback of the approach, its simplicity allows us to include in the interaction Kernel both long range (non-local) and short range interactions. Regarding the different feedback mechanisms, we can for example cite the presence of regions with increased scouring around a vegetated obstacle (non-local and negative), the sediment stabilization by roots inducing a larger critical shear stress for sediment transport (local and positive) or the decreased flow velocity due to increased roughness (local and positive). Seeding and resprouting can also be included in the positive part of the interaction Kernel as a local positive contribution to the biomass density.

When studying the stability of the neural model, we shall consider a straight-channel geometry with periodic boundary conditions in the transverse direction $\mathbf{e}_n$. Thus, alternate bars cannot be captured by the Kernel model as formulated here (the boundary introduces an asymmetry). In the longitudinal direction $\mathbf{e}_s$, we assume the channel to be infinite. For causality reasons (flow and sediment transport are mainly modified downstream of a vegetated obstacle) the Kernel functions need to satisfy the following additional condition $\mathcal{W}(s' - s, n' - n) = 0$ for $s' - s > 0$.

As in Section 3, we perform a stability analysis by perturbing a homogeneous reference state. It is therefore useful to carefully discuss homogeneous solutions of Eq. (13). Neglecting the spatial dependence of the biomass density ϕ one readily obtains the two solutions

$$\phi_0 = 0 \quad \text{and} \quad \phi_h = \phi_m + \frac{1}{\alpha_g}\hat{\hat{\mathcal{W}}}(k_s = 0, k_n = 0), \quad (14)$$

with $\hat{\hat{\mathcal{W}}}(k_s, k_n)$ the Fourier transform of the Kernel function

$$\hat{\hat{\mathcal{W}}}(k_s, k_n) = \iint \mathcal{W}(s, n)e^{ik_s s}e^{ik_n n}dsdn. \quad (15)$$

The stability of the trivial solution ϕ_0 depends on the integral of the Kernel. If the negative couplings are very strong one may obtain a non-physical negative value $\phi_h < 0$ and accordingly ϕ_0 becomes stable. In other situations, the trivial solution is unstable and ϕ_h can be interpreted as a modified carrying capacity, increased or decreased depending on whether positive or negative couplings dominate.

Following [43] we separate the positive (regions with reduced shear stress) and the negative (regions with increased flow velocity and/or TKE) part of the Kernel $\mathcal{W} = W_+ + W_-$ and assume that protective effects of vegetation (e.g. reduction of the local shear stress and sediment stabilization by roots) have a much shorter range than the characteristic size of the region around the obstacle with perturbed flow (for a simple estimation of the size of the obstacle scour, see [44]). Performing an expansion valid for short-ranged positive feedback, we can rewrite Eq. (13) in the following form:

$$\frac{\partial \phi}{\partial t} = \alpha_g \phi\left(\phi_m + \frac{A}{\alpha_g} - \phi\right) + B\partial_s\phi + D_n\partial_n^2\phi + D_s\partial_s^2\phi + \phi * W_-. \quad (16)$$

In the last term we have introduced the star product as a shorthand notation for the convolution product. The expansion of the positive part of the Kernel yields

$$A = \iint W_+(s', n')ds'dn' \quad (17a)$$

$$B = \iint s' W_+(s', n') ds' dn' \tag{17b}$$

$$D_{\{s,n\}} = \iint \{s', n'\}^2 W_+(s', n') ds' dn'. \tag{17c}$$

The term (17a) can be included within an effective carrying capacity $\phi_m + \frac{A}{\alpha_g}$. Due to the symmetry of the flow around obstacles we do not have a first order derivative regarding the transverse direction $\mathbf{e}_n$. In the longitudinal direction however, the asymmetry in the flow direction results in a non-zero first order term. This term can describe the sheltering effect behind a (permeable) vegetated obstacle. We stop the expansion with the second order term of the Kernel expansion, which takes the form of a diffusion term. In principle, one can expect different values for the longitudinal and transverse diffusion coefficients $D_{\{s,n\}}$ due to the asymmetry introduced by the flow. The fact that any short-ranged positive coupling takes the form of a diffusion justifies a posteriori the introduction of biomass diffusion in Eqs. (3) and (9).

In order to study the stability of the homogeneous solution (14), we apply the method developed by [45]. We use the following perturbation from the homogeneous solution ϕ_h:

$$\varepsilon\, e^{\omega t + i k_s s + i k_n n} + cc. \tag{18}$$

We introduced *cc.* a shorthand notation for the complex conjugate and ε a small perturbation parameter (linear stability analysis corresponds to a first order expansion in ε). Similar to the procedure from the previous Section, ω gives the growth rate of the perturbation and the mode (characterized by the longitudinal and transverse wavenumbers k_s and k_n respectively) with the largest positive growth rate is the most unstable (asymptotically dominates the other modes). In case no mode satisfies $\max(k_{s,n}) > 0$ *and* $\omega > 0$ then the homogeneous solution is stable, which corresponds either to a homogeneous vegetation cover or to the situation with no vegetation populating the riverbed. Note that only one of the wavenumbers needs to be strictly positive in order to have patterns. As a result, one obtains [43] the general condition for the onset of patterns

$$-k_n^2 - \frac{D_s}{D_n} k_s^2 - \frac{2}{A + \alpha\phi_m}\left[\hat{\mathcal{W}}_-(0,0) - \mathrm{Re}(\hat{\mathcal{W}}_-(k_s, k_n))\right] > 1. \tag{19}$$

This condition can be generalized to any functional dependence of the negative part of the Kernel W_-.

For a field study on sediment deposition and scouring around vegetated obstacles of the type found in the Marshall River (river red gums, see Fig. 1, upper panel and [22,23]), we refer to [20]. In order to model the region with increased scouring around vegetated obstacles observed by [20], we fix now the negative part of the Kernel by assuming the following form:

$$W_-(s, n) = -\alpha_d\, \theta(s) e^{-\left(\frac{s}{l_s}\right)^2 + \left(\frac{n}{l_n}\right)^2} \tag{20}$$

with $\theta(s)$ the Heaviside function [46] and α_d a rate of biomass mortality. The lengths L_s and L_n give the characteristic size of the region with an increased scouring in the longitudinal and transverse direction respectively. From the general condition (19), we can now derive specific conditions for the emergence of anabranching patterns. Before turning to the stability analysis of Eq. (13), we show in Fig. 6 the results of a simulation of the dynamics resulting from Eq. (13). One readily notices that the model is able to reproduce the emergence of well-defined ridge patterns starting from a random vegetation cover. Interestingly, we see that first (transition from panel A to panel B) the width w_i and the length l_i of the vegetated clusters increase together with the distance d_i between them. In a second stage (transition from panel B to panel C), we see a coalescing and streamlining of the clusters leading to an increase of l_i with almost unchanged w_i and d_i.

Let us begin with the condition for pattern stability in the longitudinal direction $\mathbf{e}_s$. From the Hessian of $\omega(k_s, k_n)$ we obtain a very

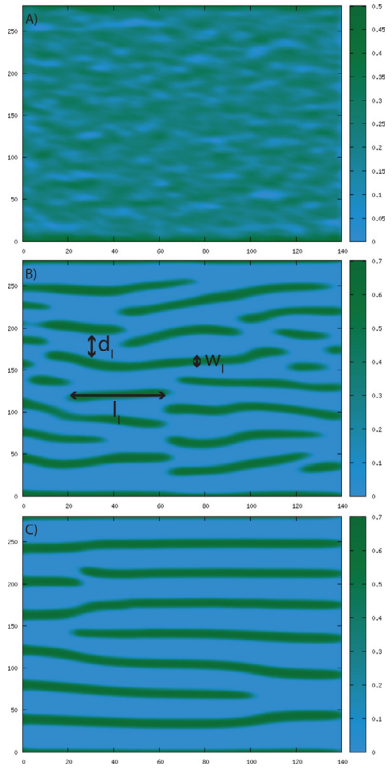

Fig. 6. Example simulation of the evolution of the biomass density (carrying capacity $\phi_m = 1$) using the Kernel model for a 280 by 140 grid. From an initial random vegetation cover (upper panel) the vegetation organizes itself into a regular periodic pattern (lower panel). The variables l_i, w_i and d_i denote the length of a vegetation cluster, its width and the average distance to the neighboring clusters respectively.

simple condition on the diffusion times $t_{s,n} = L_{s,n}^2 / D_{s,n}$ necessary in order for $k_s = 0$ to dominate (maximal ω):

$$t_n > t_s. \tag{21}$$

Eq. (21) can be interpreted as transverse patterns remaining stable in the longitudinal direction for a faster spreading of vegetation in the region sheltered from the flow than in the transverse direction. In other words, Eq. (21) is a prerequisite for the emergence of stable ridges such as the ones observed in the Marshall River (Fig. 1, upper panel). From now on we assume that (21) is satisfied, as it is for example the case if D_s is large enough. Two conditions emerge then for transverse patterns: the first one is related to the existence of a maximum for $\omega(0, k_n)$ at a finite wavenumber k_n^{max}

$$\frac{\alpha_d (A + \alpha_g \phi_m)}{D_n^2} L_n^3 L_s \pi > 8. \tag{22}$$

The second one requires that the maximum yields a strictly positive value of the instability growth rate $\omega(k_n^{max}) > 0$

$$\frac{\alpha_d L_s L_n \pi}{2 D_n} - \frac{4 D_n}{(A + \alpha_g \phi_m) L_n^2}\left[1 - \log\left(\frac{8 D_n^2}{\alpha_d (A + \alpha_g \phi_m) L_n^3 L_s \pi}\right)\right] > 1. \tag{23}$$

Finally, the selected maximal growth rate occurs for

$$k_n^{max} = \frac{2}{L_n}\sqrt{\frac{D_n}{(A + \alpha_g \phi_m)} \mathrm{Log}\left(\frac{\alpha_d (A + \alpha_g \phi_m) L_n^3 L_s \pi}{8 D_n^2}\right)}. \tag{24}$$

As long as the three conditions (21)–(23) are satisfied, the homogeneous solution is unstable and evolves towards stable ridge patterns. Interestingly, the Kernel parameter B introduced in (16) is not present in any of the three conditions for the emergence of patterns. In the same direction, B does not modify the selected wavenumber

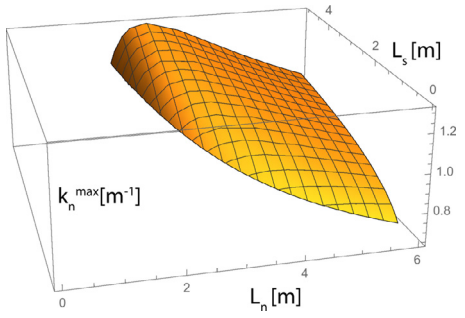

Fig. 7. Wavenumber $k_n^{max} = \frac{2\pi}{\lambda}$ quantifying the pattern wavelength λ, varying the range of the interaction Kernel $L_{s,n}$ for fixed $A + \alpha_g \phi_m = 2\,\mathrm{day}^{-1}$, $D_n = 4\,\mathrm{m}^2\mathrm{day}^{-1}$ and $\alpha_d = 1\,\mathrm{day}^{-1}$.

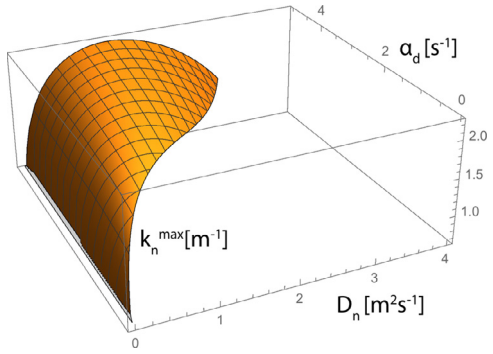

Fig. 8. Wavenumber $k_n^{max} = \frac{2\pi}{\lambda}$ quantifying the pattern wavelength λ, varying the diffusion coefficient of vegetation D_n and the vegetation mortality rate α_d for fixed $A + \alpha_g \phi_m = 2\,\mathrm{day}^{-1}$ and $L_s = 3L_n = 3\,\mathrm{m}$.

k_n^{max} (purely imaginary contribution). Note also that while our approach is able to predict the emergence of the instability in the linear stage and the initial pattern wavelength, the wavenumber k_n^{max} (24) may change if the perturbation reaches the point where non-linear effects cannot be neglected anymore. Keeping this limitation in mind, we use in the following our effective model to discuss the effect of changes in the range and intensity of the interactions present in the ecomorphodynamic model (13).

In Fig 7, we plot the transverse wavenumber with the maximal instability k_n^{max} varying the transverse and longitudinal range of the negative part of the Kernel (L_n and L_s respectively). No instability takes place for small range of W_- along (L_s) or transverse (L_n) to the flow. Increasing the range of the negative part of the Kernel in the longitudinal direction increases k_n^{max} (or decreases the wavelength $2\pi/k_n^{max}$). The dependence of k_n^{max} on the range in the transverse direction is however non-monotonic: one observes first an increase of k_n^{max} and then a decrease (larger wavelength and larger distance between the obstacles). The initial increase of the wavenumber as a function of the range in the transverse direction may be seen as a way of averaging out the long-range negative part of the Kernel.

In Fig. 8, we vary the transverse diffusion coefficient D_n and the vegetation mortality rate α_d while keeping the other model parameters constant. The transverse wavenumber k_n^{max} increases monotonically with α_d. And, as it was the case for $L_{s,n}$, patterns are only present when α_d is above a certain threshold. For the transverse diffusion coefficient D_n however the dependence of k_n^{max} is non-monotonic and patterns are present as soon as $D_n > 0$ (no threshold).

5. Discussion

The two approaches we proposed in Sections 3 and 4 should be seen in their complementarity. The physically-based approach (Section 3) is in principle preferable since it allows for a direct mechanistic interpretation and parameterization. We expect this approach to work best when considering the perturbation of a homogeneous cover of grass or shrubs, as for example to model the situation represented in the lower panel of Fig. 1. The complexity of the feedback between riparian vegetation and morphodynamics (sediment transport and flow) makes a complete detailed description of the involved processes hopeless in the presence of more complex vegetated obstacles, as it is for example the case in the situation represented in the upper panel of Fig. 1. Due to the use of a lumped model, the discussion on the role of the different components of the Kernel model should be taken with caution. We however believe that this type of model can contribute to the qualitative understanding of the processes involved in the organization of complex vegetated obstacles and the formation of anabranching patterns.

An explanation for the inability of our physically-based model to reproduce ridges with a length-to-width asymmetry larger than 10 could reside in the limitations of the model used to describe flow-vegetation interactions and possibly in the use of linear stability analysis. While it is reasonable to expect the simple description involving bed-roughness changes and flow-induced mortality to reproduce the onset of the instability, at some point the amplitude of the patterns may result either in a more complex disturbance of the flow (to be eventually captured by an effective model) or to a shift of the pattern wavelength due to the non-linearity of Eqs. (4)–(9).

For the physical model we focused on a particular vegetation model and included simple couplings between morphodynamics and vegetation. This model can be extended to include effects relevant for the precise situation one wants to model. In particular, we can readily take into account in Eq. (5) the volume of the plants present in the section $\frac{d^2 Y \pi \phi}{4}$. Similarly, while we considered rigid vegetation in Eqs. (4) and (9), accounting for the streamlining of the plants would result in a shear stress induced by the biomass proportional to $||\mathbf{U}||^p$ with $1 \leq p \leq 2$ ($p = 1$ corresponds to perfectly flexible vegetation). Including a more realistic description of the sediment transport law (7) (valid also for lower shear stress) is in principle possible. Stabilization of sediment by roots could for example be expressed by a change in the critical bed stress for incipient sediment motion [47]. Working with thresholds would however preclude an analytical treatment such as the one performed in Section 3. In this regard, a numerical approach [48] could then be used to investigate threshold effects.

For both the physically-based approach and the effective model, vegetated patterns are the product of the interplay between positive and negative feedbacks: locally the biomass mortality can be either increased or reduced due to the presence of neighboring vegetation. In the physically-based approach the positive and negative feedbacks are a combination of the changes in roughness induced by the biomass (local velocity can be reduced or increased locally due to flow deflection) and the flow-induced mortality. In the Kernel model however, we explicitly separated positive and negative feedbacks.

6. Summary and conclusion

We presented an analytical modeling framework for the co-evolution of vegetation and riverbed morphology. We first discussed the importance of flow intermittency in allowing for strong feedback between biomass and morphodynamics. Flow intermittency can either characterize the whole channel (ephemeral river, see for example Fig. 1, upper panel) or be the result of the location within the riverbed (river bar, see Fig. 1, lower panel). We then showed that the dynamics of a slowly evolving vegetated channel can be described using constant-flow equations. Important in order to observe a strong feedback between ecological processes and morphodynamics is a riverbed consisting of low-cohesive sediment: sediment deposition and scouring play a significant part in determining the fate of riverbed vegetation (survival or uprooting, see [13]).

We proposed a physically-based model as a prototype for the interplay between vegetation and morphodynamics. By performing

a linear stability analysis we studied the longitudinal vs. transverse asymmetry of vegetation-associated patterns. We showed that although an instability towards multiple bars is possible in the presence of vegetation, single-threaded configuration (alternate bars or uniform conditions) are favored.

In order to model situations with complex vegetated obstacles we proposed to use a lumped approach for the evolution of riparian vegetation. The presence of obstacles can locally increase the flow velocity and/or the TKE resulting in obstacle-induced scouring. Conversely, on the lee-side of permeable obstacles (for example a bush with significant bleed flow) deposition of sediment and seeds can be increased. By performing a stability analysis of the Kernel model, we showed that this type of model is able to reproduce a stable ridge pattern. We discussed the domain where the pattern can be observed and its wavelength as function of the characteristics (range and intensity) of the interactions between vegetated obstacles located at different positions in a channel. Remarkably, we obtained a non-monotonic dependence of the pattern wavelength on the range of the feedback in the transverse direction. For certain parameters, we identified windows in the parameter space where patterns can be observed, supporting our working hypothesis that a non-trivial interplay between vegetation and morphodynamics can be observed only in a certain parameter and timescale window (Section 2). Central to our results is the necessity of having both positive and negative interactions in order to be able to reproduce patterns.

The insight from controlled flume experiments, together with field surveys would be particularly helpful at this point. While the quantification of the effects induced by the presence of riparian vegetation in rivers has attracted much attention recently, we believe that experimental and field works in the perspective of a lumped description of the positive *and* negative interactions involving complex vegetated obstacles [1,12,20] could also help advancing the understanding of river geomorphological trajectories.

Acknowledgements

This work has been completed in the ambit of the Swiss National Science Foundation project REMEDY (Grant number PP00P2-153028/1).

References

[1] Gurnell AM, Bertoldi W, Corenblit D. Changing river channels: the roles of hydrological processes, plants and pioneer fluvial landforms in humid temperate, mixed load, gravel bed rivers. Earth-Sci Rev 2012;111(1–2):129–41. http://dx.doi.org/10.1016/j.earscirev.2011.11.005.

[2] Tal M, Paola C. Dynamic single-thread channels maintained by the interaction of flow and vegetation. Geology 2007;35(4):347–50. http://dx.doi.org/10.1130/G23260A.1.

[3] Perona P, Molnar P, Crouzy B, Perucca E, Jiang Z, McLelland S, Wüthrich D, Edmaier K, Francis R, Camporeale C, Gurnell A. Biomass selection by floods and related timescales: part 1. experimental observations. Adv Water Resour 2012;39:85–96. http://dx.doi.org/10.1016/j.advwatres.2011.09.016.

[4] Camporeale C, Perucca E, Ridolfi L, Gurnell AM. Modeling the interactions between river morphodynamics and riparian vegetation. Rev Geophys 2013;51(3):379–414. http://dx.doi.org/10.1002/rog.20014.

[5] Solari L, Van Oorschot M, Belletti B, Hendriks D, Rinaldi M, Vargas-Luna A. Advances on modelling riparian vegetation—hydromorphology interactions. River Res Appl 2015. http://dx.doi.org/10.1002/rra.2910.

[6] Hickin E. Vegetation and river channel dynamics. Can Geogr 1984;28(2):111–26. http://dx.doi.org/10.1111/j.1541-0064.1984.tb00779.x.

[7] Simon A, Bennet SJ, editor. Riparian vegetation and fluvial geomorphology. Water Science and Application Series, vol. 8. Washington, DC: American Geophysical Union; 2004. http://dx.doi.org/10.1029/WS008.

[8] Gorrick S, Rodriguez JF. Sediment dynamics in a sand bed stream with riparian vegetation. Water Resour Res 2012;48(2). http://dx.doi.org/10.1029/2011WR011030.

[9] Zong L, Nepf H. Flow and deposition in and around a finite patch of vegetation. Geomorphology 2010;116:363–72. http://dx.doi.org/10.1016/j.geomorph.2009.11.020.

[10] Perona P, Molnar P, Savina M, Burlando P. An observation-based stochastic model for sediment and vegetation dynamics in the floodplain of an alpine braided river. Water Resour Res 2009;45:W09418. http://dx.doi.org/10.1029/2008WR007550.

[11] van Dijk WM, Teske R, van de Lageweg WI, Kleinhans MG. Effects of vegetation distribution on experimental river channel dynamics. Water Resour Res 2013;49(11):7558–74. http://dx.doi.org/10.1002/2013WR013574.

[12] Gurnell AM, Petts GE. Trees as riparian engineers: the Tagliamento River, Italy. Earth Surf Process Landf 2006;31:1558–74. http://dx.doi.org/10.1002/esp.1342.

[13] Edmaier K, Burlando P, Perona P. Mechanisms of vegetation uprooting by flow in alluvial non-cohesive sediment. Hydrol Earth Syst Sci 2011;15(5):1615–27. http://dx.doi.org/10.5194/hess-15-1615-2011.

[14] Seminara G. Fluvial sedimentary patterns. Annu Rev Fluid Mech 2010;42:43–66. http://dx.doi.org/10.1146/annurev-fluid-121108-145612.

[15] Engelund F, Fredsoe J. Sediment ripples and dunes. Annu Rev Fluid Mech 1982;14(1):13–37. http://dx.doi.org/10.1146/annurev.fl.14.010182.000305.

[16] Lanzoni S, Siviglia A, Frascati A, Seminara G. Long waves in erodible channels and morphodynamic influence. Water Resour Res 2006;42(6). http://dx.doi.org/10.1029/2006WR004916.

[17] Engelund F, Skovgaard O. On the origin of meandering and braiding in alluvial streams. J Fluid Mech 1973;57:289–302. http://dx.doi.org/10.1017/S0022112073001163.

[18] Ikeda S, Parker G, Sawai K. Bend theory of river meanders. part 1. linear development. J Fluid Mech 1981;112:363–77. http://dx.doi.org/10.1017/S0022112081000451.

[19] Camporeale C, Perona P, Porporato A, Ridolfi L. Hierarchy of models for meandering rivers and related morphodynamic processes. Rev Geophys 2007;45(1). http://dx.doi.org/10.1029/2005RG000185.

[20] Nakayama K, Fielding C, Alexander J. Variations in character and preservation potential of vegetation-induced obstacle marks in the variable discharge Burdekin River of north Queensland, Australia. Sediment Geol 2002;149(4):199–218. http://dx.doi.org/10.1016/S0037-0738(01)00173-7.

[21] Rodrigues S, Bréhéret J-G, Macaire J-J, Greulich S, Villar M. In-channel woody vegetation controls on sedimentary processes and the sedimentary record within alluvial environments: a modern example of an anabranch of the River Loire, France. Sedimentology 2007;54(1):223–42. http://dx.doi.org/10.1111/j.1365-3091.2006.00832.x.

[22] Tooth S, Nanson GC. The role of vegetation in the formation of anabranching channels in an ephemeral river, Northern plains, arid central Australia. Hydrol Process 2000;14:3099–117. http://dx.doi.org/10.1002/1099-1085(200011/12)14:16/17<3099::aid-hyp136>3.0.CO;2-4.

[23] Tooth S, Nanson GC. Forms and processes of two highly contrasting rivers in arid central Australia, and the implications for channel-pattern discrimination and prediction. Geol Soc Am Bull 2004;116(7–8):802–16. http://dx.doi.org/10.1130/B25308.1.

[24] Nanson GC, Tooth S, Knigthon D. A global perspective on dryland rivers: perceptions, misconceptions and distinctions. Dryland rivers: hydrology and geomorphology of semi-arid channels. Bull LJ, Kirby MJ, editors, New York: John Wiley and Sons, Ltd.; 2002. ISBN: 978-0-471-49123-1.

[25] Huang HQ, Nanson GC. Why some alluvial rivers develop an anabranching pattern. Water Resour Res 2007;43:W07441. http://dx.doi.org/10.1029/2006WR005223.

[26] Jansen JD, Nanson GC. Functional relationship between vegetation, channel morphology, and flow efficiency in an alluvial (anabranching) river. J Geophys Res 2010;115:F07441. http://dx.doi.org/10.1029/2010JF001657.

[27] Camporeale C, Perona P, Ridolfi L. Hydrological and geomorphological significance of riparian vegetation in drylands. Dryland ecohydrology. D'Odorico P, Porporato A, editors. Dordrecht, The Netherlands: Springer; 2006. http://dx.doi.org/10.1007/1-4020-4260-4_10.

[28] Crouzy B, Perona P. Biomass selection by floods and related timescales: part 2. stochastic modeling. Adv Water Resour 2012;39:97–105. http://dx.doi.org/10.1016/j.advwatres.2011.09.018.

[29] Baptist MJ, Babovic V, Uthurburu JR, Keijzer M, Uittenbogaard RE, Mynett A, Verwey A. On inducing equations for vegetation resistance. J Hydraul Res 2007;45(4):435–50. http://dx.doi.org/10.1080/00221686.2007.9521778.

[30] Crouzy B, Edmaier K, Pasquale N, Perona P. Impact of floods on the statistical distribution of riverbed vegetation. Geomorphology 2013;202:51–8. http://dx.doi.org/10.1016/j.geomorph.2012.09.013.

[31] Verhulst P-F. Recherches mathématiques sur la loi d'accroissement de la population. Nouv Mém Acad R Sci B-Lett Brux 1845;18:1–42.

[32] Perona P, Crouzy B, McLelland S, Molnar P, Camporeale C. Ecomorphodynamics of rivers with converging boundaries. Earth Surf Process Landf 2014;39(12):1651–62. http://dx.doi.org/10.1002/esp.3614.

[33] Federici B, Seminara G. On the convective nature of bar instability. J Fluid Mech 2003;487:125–45. http://dx.doi.org/10.1017/S0022112003004737.

[34] Colombini M, Seminara G, Tubino M. Finite-amplitude alternate bars. J Fluid Mech 1987;181:213–32. http://dx.doi.org/10.1017/S0022112087002064.

[35] Meyer-Peter E, Müller R. Formulas for bed-load transport. In: Proceedings of the 2nd meeting of the international association for hydraulic structures research; 1948. p. 39–64.

[36] Borgogno F, D'Odorico P, Laio F, Ridolfi L. Mathematical models of vegetation pattern formation in ecohydrology. Rev Geophys 2009;47(1). http://dx.doi.org/10.1029/2007RG000256.

[37] D'Odorico P, Laio F, Porporato A, Ridolfi L, Barbier N. Noise-induced vegetation patterns in fire-prone savannas. J Geophys Res: Biogeosci 2007;112(G2). http://dx.doi.org/10.1029/2006JG000261.

[38] Tealdi S, Camporeale C, Ridolfi L. Inter-species competition–facilitation in stochastic riparian vegetation dynamics. J Theor Biol 2013;318(0):13–21. http://dx.doi.org/10.1016/j.jtbi.2012.11.006.

[39] Wong M, Parker G. Reanalysis and correction of bed-load relation of Meyer-Peter and Müller using their own database. J Hydraul Eng 2006;132(11):1159–68. http://dx.doi.org/10.1061/(ASCE)0733-9429(2006)132:11(1159).
[40] Camporeale C, Ridolfi L. Nonnormality and transient behavior of the de Saint-Venant-Exner equations. Water Resour Res 2009;45(8). http://dx.doi.org/10.1029/2008WR007587.
[41] Baerenbold F, Crouzy B, Perona P. Stability analysis of ecomorphodynamic equations. Water Resour Res 2015.in preparation.
[42] Davies NS, Gibling MR. Evolution of fixed-channel alluvial plains in response to Carboniferous vegetation. Nat Geosci 2011;4(9):629–33. http://dx.doi.org/10.1038/ngeo1237.
[43] Crouzy B, D'Odorico P, Perona P. Ecomorphodynamic conditions for the emergence of river anabranching patterns. In: River flow 2014. The Netherlands: CRC Press/Balkema Leiden; 2014. http://dx.doi.org/10.1201/b17133-151.
[44] Melville BW, Sutherland AJ. Design method for local scour at bridge piers. ASCE J Hydraul Div 1988;114(10):1210–26. http://dx.doi.org/10.1061/(ASCE)0733-9429(1988)114:10(1210).
[45] Turing AM. The chemical basis of morphogenesis. Philos Trans R Soc Lond Ser B: Biol Sci 1952;237(641):37–72. http://dx.doi.org/10.1098/rstb.1952.0012.
[46] Abramowitz M, Stegun IA. Handbook of mathematical functions with formulas, graphs, and mathematical tables, New York: Dover; 1972. ISBN: 0486612724.
[47] Pasquale N, Perona P. Experimental assessment of riverbed sediment reinforcement by vegetation roots. In: Proceedings of the 7th international conference on fluvial hydraulics (River Flow); 2014. http://dx.doi.org/10.1201/b17133-77.
[48] Bertoldi Walter, Siviglia Annunziato, Tettamanti Stefano, Toffolon Marco, Vetsch David, Francalanci Simona. Modeling vegetation controls on fluvial morphological trajectories. Geophys Res Lett 2014;41(20):7167–75. http://dx.doi.org/10.1002/2014GL061666.